ADVANCED FUNCTIONAL MATERIALS

Supporting Information

for *Adv. Funct. Mater.*, DOI 10.1002/adfm.202401658

The Multiphasic Teeth of *Chiton Articulatus*, an Abrasion-Resistant and Self-Sharpening Tool for Hard Algae Collection

*Devis Montroni, Ezra Sarmiento, Ruoheng Zhao, Phani Saketh Dasika, John Michael Connolly, Richard Wuhrer, Yugang Zhang, Mikhail Zhernenkov, Taifeng Wang, Brenda Paola Ramirez-Santana, Leigh Sheppard, Omar Hernando Avila-Poveda, Atsushi Arakaki, Michiko Nemoto, Pablo Zavattieri and David Kisailus**

Supporting Information

The multiphasic teeth of Chiton articulatus, an abrasion-resistant and self-sharpening tool for hard algae collection.

Devis Montroni, Ezra Sarmiento, Ruoheng Zhao, Phani Saketh Dasika, John Michael Connolly, Richard Wuhrer, Yugang Zhang, Mikhail Zhernenkov, Taifeng Wang, Brenda Paola Ramirez-Santana, Leigh Sheppard, Omar Hernando Avila-Poveda, Atsushi Arakaki, Michiko Nemoto, Pablo Zavattieri, and David Kisailus*.

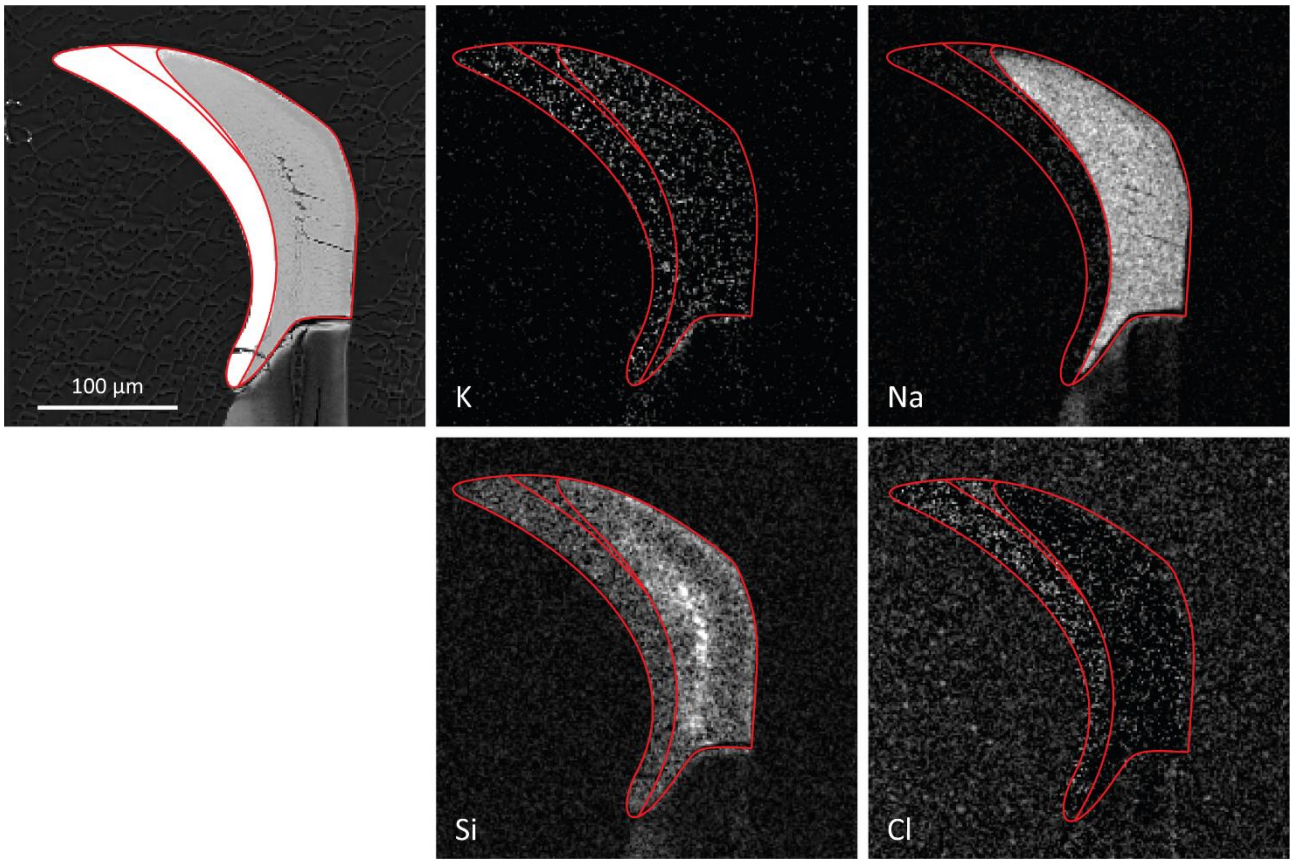

Figure S1: EDS-SEM analysis of a mature tooth longitudinal section revealed the distribution of different minor elements. A red line profile defines the three different regions in the tooth.

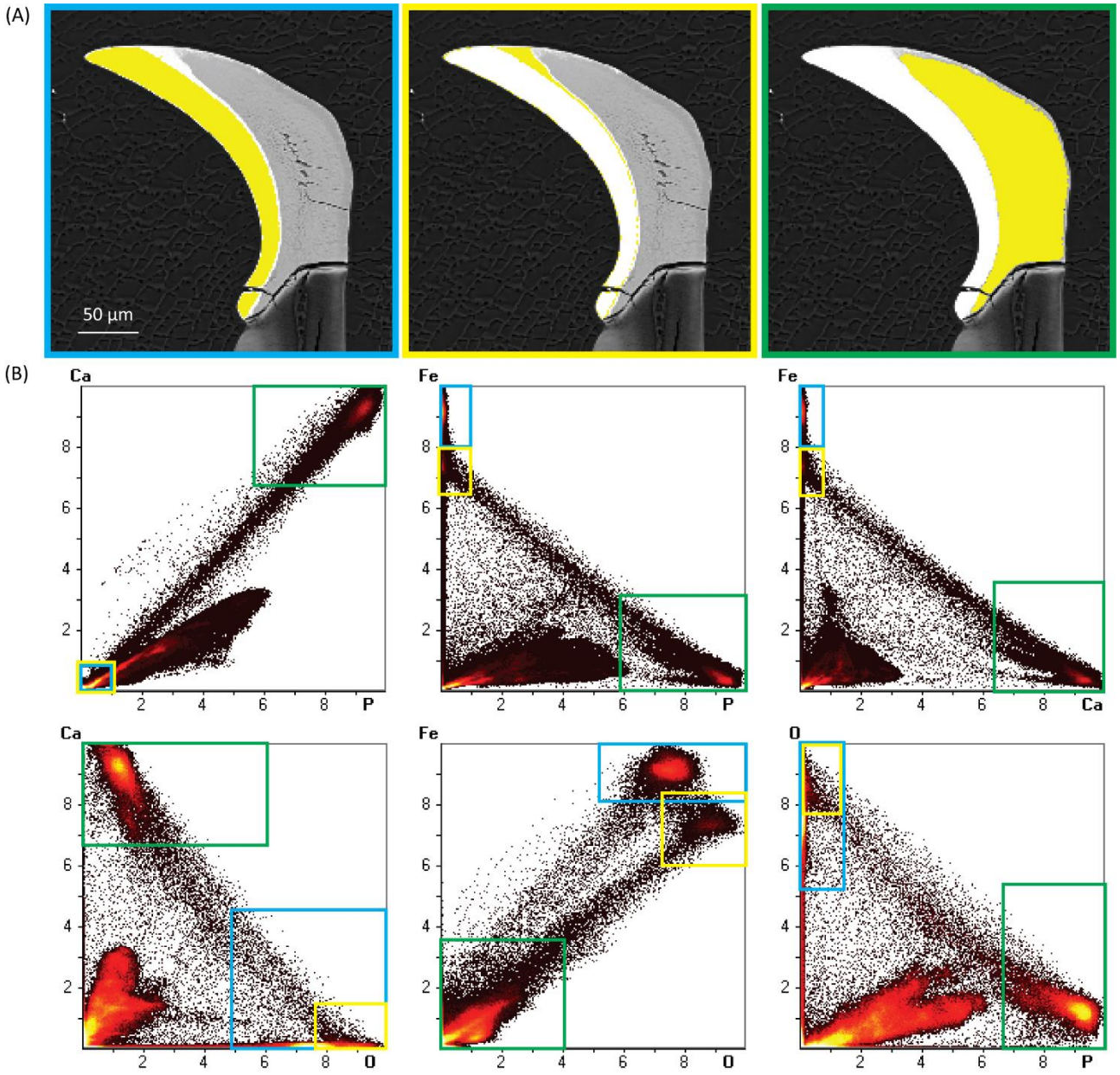

Figure S2: EDS correlation graphs. (A) Identification of the pixels in the SEM micrographs from which the corresponding correlation graphs are calculated. (B) Correlation graphs of different element couples. Light blue squares identify the points corresponding to Region 1, yellow squares identify Region 2, and green squares identify Region 3. The remaining non-specified points are related to the stylus and the resin used for the sample embedding.

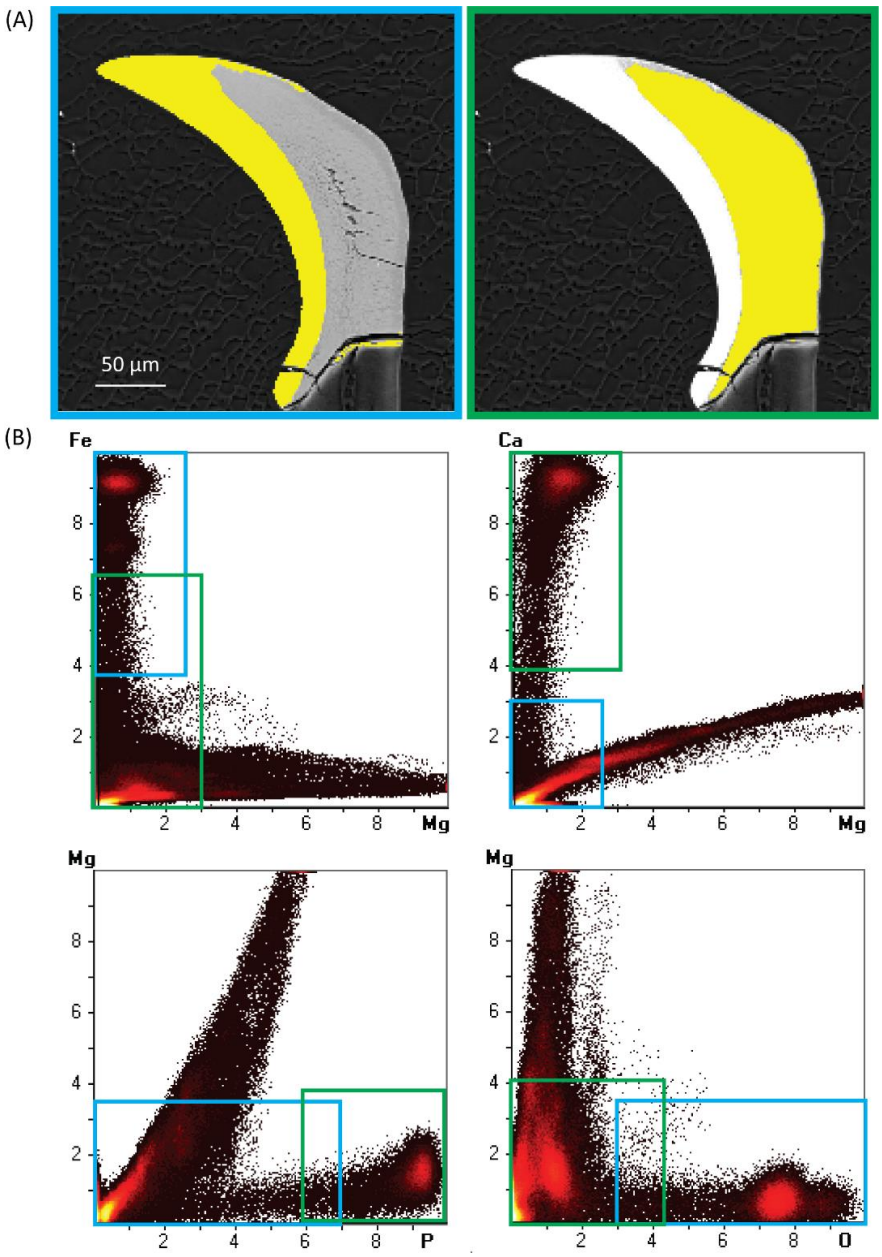

Figure S3: EDS correlation graphs describing the relationship between Fe and O with Mg. (A) Identification of the pixels in the SEM micrographs from which the corresponding correlation graphs are calculated. (B) Correlation graphs of different elements coupled with Mg. Light blue squared identify the points corresponding to Region 1 and 2. The remaining non-specified points are related to the stylus and resin composition. No specific range was attributed to Region 3.

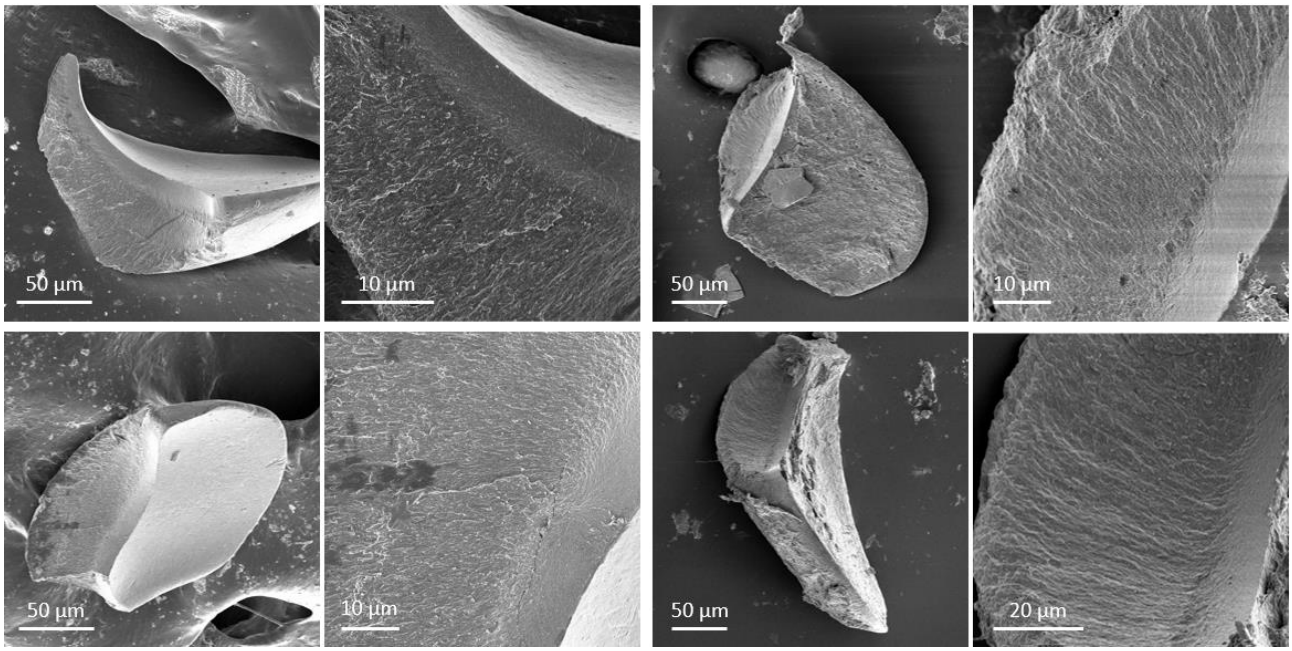

Figure S4: SEM of different broken tooth tips showing a concave cleavage surface, following the orientation of the mineral phase in the tooth. For each sample, two magnifications are reported. The higher magnifications show how the maximum of the concave surface is always located at the interface between the particles and the lamellae region.

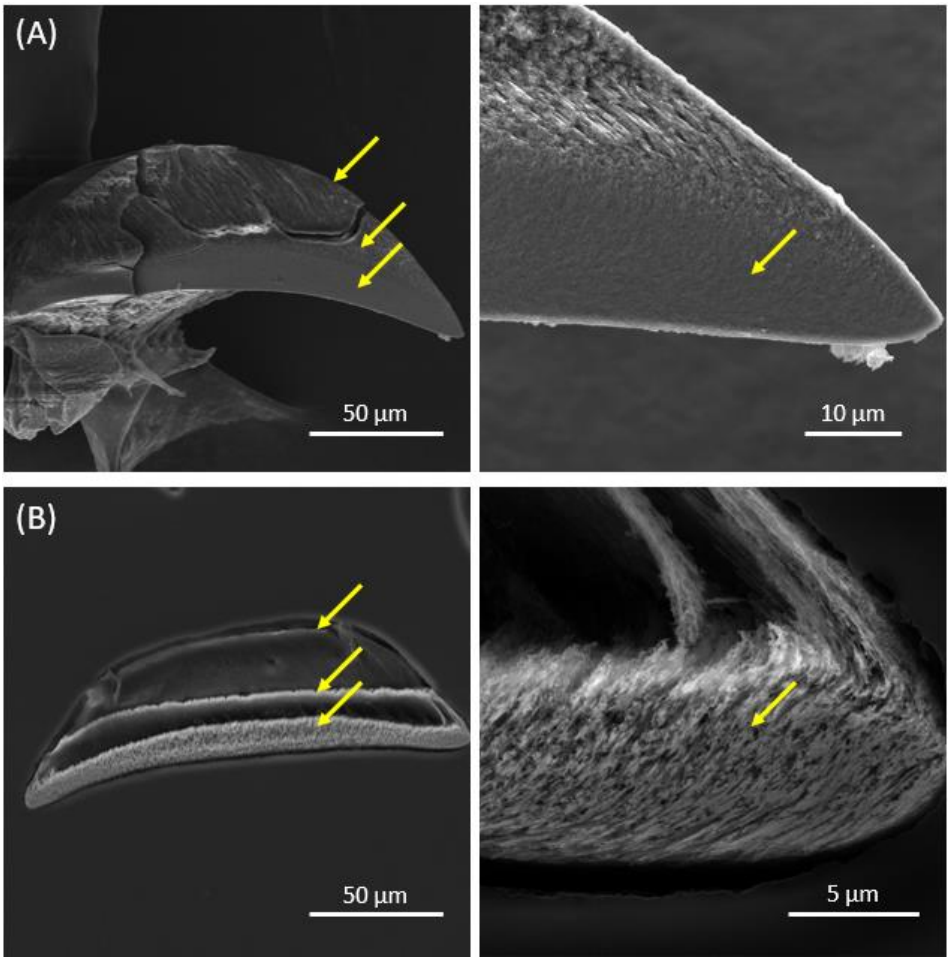

Figure S5: (A) Broken transversal section of a mature tooth at two different magnifications. (B) SEM images at two different magnifications of the transversal section of a polished tooth encased in epoxy resin showing and fully demineralized using oxalic acid 0.3 M, the images show the organic phase. Yellow arrows identify analog points in the mineralized and demineralized samples showing where the organic phase should be located.

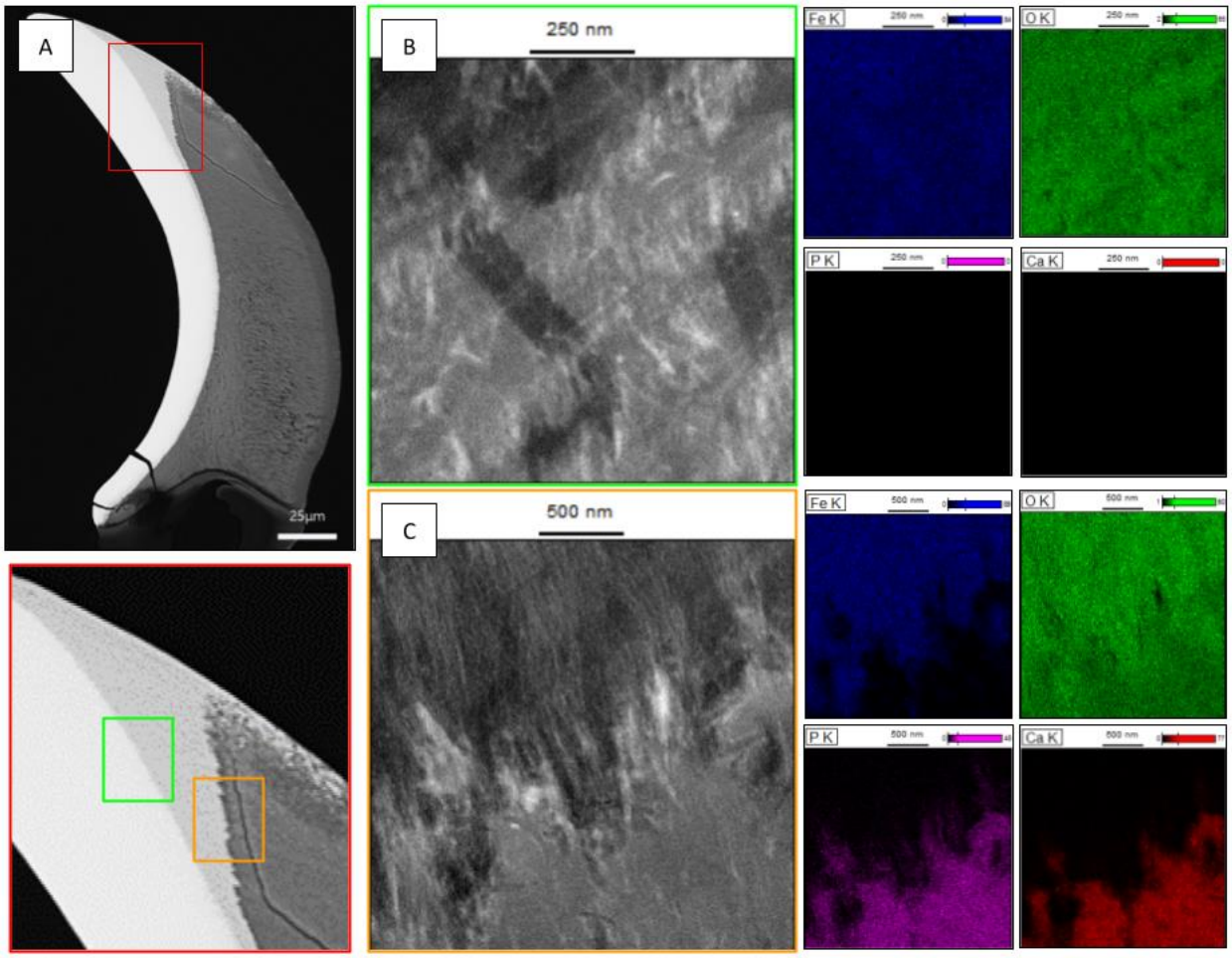

Figure S6: (A) BSE of the chiton tooth with EDS of the interface between (B) Regions 1 and 2 and (C) Regions 2 and 3. Regional differences in the concentrations of Fe, O, P, and C are corroborated with SAED in Figure 6 to characterize the phases present in each region.

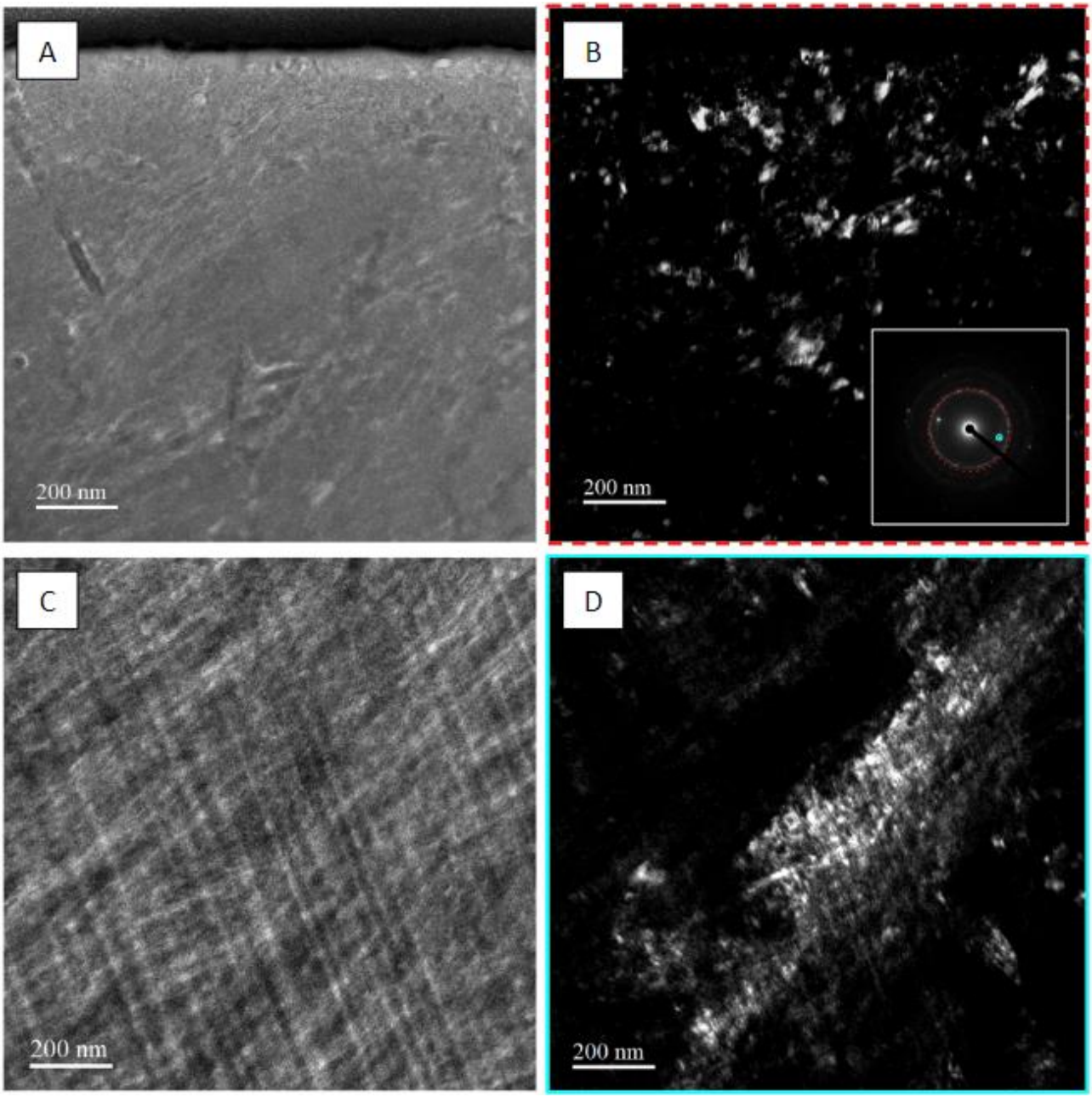

Figure S7: TEM of the (A) hydroxyapatite and (C) lepidocrocite regions with DF highlighting (B) nano-crystalline (002) hydroxyapatite and (D) larger lepidocrocite needles in their respective areas.

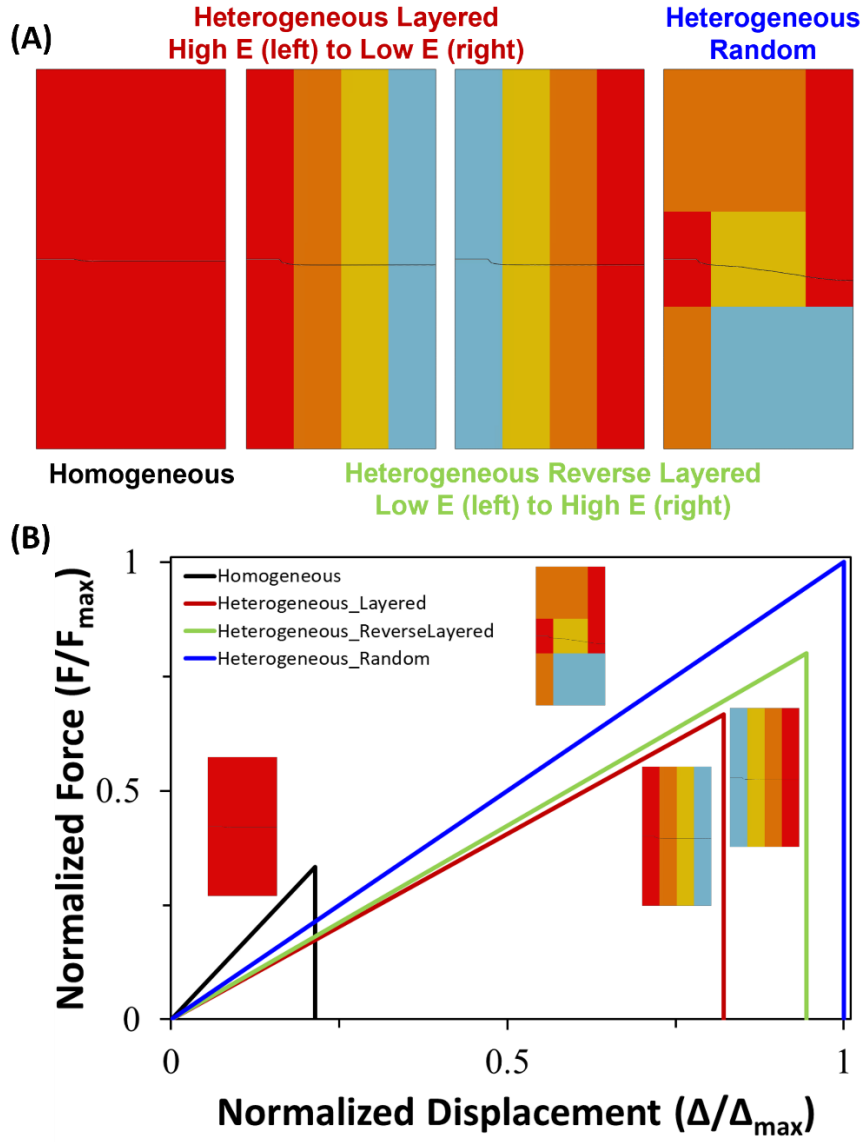

Figure S8: XFEM crack propagation across single-edge cracked rectangular plate undergoing mode-1 fracture. (A) Crack propagation trajectories across four cases of material gradients - homogeneous, heterogeneous layered with high Young's Modulus (E) to low E (left to right), reverse heterogeneous layered with low E to high E (left to right), and heterogeneous randomly layered. (B) Normalized load versus displacement plots for all four cases of tensile tests under mode-1 fracture.

From S8, we can clearly see that the trajectory of the crack is dependent on the material distribution, and furthermore, the case of randomly distributed material gradient suggests that the crack prorogation can be controllably programmed to follow a set path or at least have a predictable path. The load-displacement plots are as expected for brittle failure and are consistent in terms of stiffness with the material with maximum average E having the highest stiffness and peak load. The maximum displacement reached before failure is proportional to the length of the crack path.

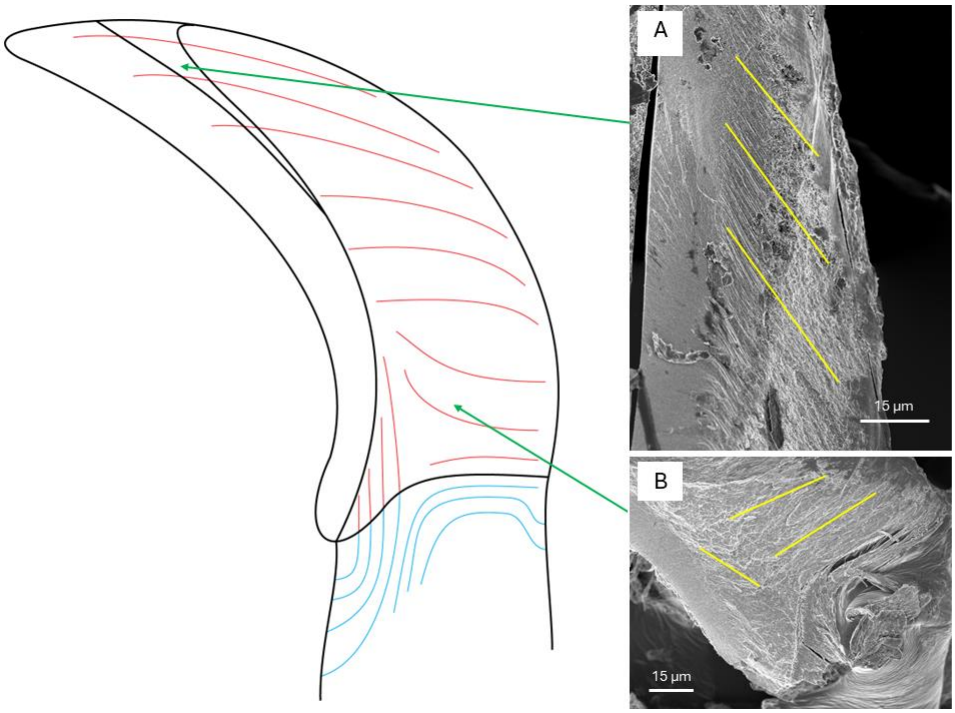

Figure S9: Schematic representing directions of lamellae within the tooth of *C. articulatus*. The change in lamellar orientation between the upper (A) and lower (B) portions of the tooth may lead to oriented crack growth and propagation in the direction of these lamellae and rods.

Figure S10: Topographic scan planes taken from Figure 6 and overlaid with selected average Py ranges calculated using values for E and H, as obtained from nanoindentation. Overall wearability of the tooth decreases as a function of height leading to the conclusion that there would be a preferential self-sharpening effect as rasping occurs.

	O	Fe	Ca	P	Mg	Na	Si

Region 1	**59%**	**40%**	0.1%	0.02%	0.3%	0.2%	0.3%
Region 2	**65%**	**33%**	0.5%	0.5%	0.3%	0.4%	0.3%
Region 3	**47%**	3.3%	**30%**	**17%**	0.7%	1.6%	0.4%

Table S1: Approximate atomic percentages of the main elements present in the three main regions of the tooth as demonstrated by EDS. The presence of the claimed crystal phases is supported by the relative amount of the elements reported in the EDS if it is considered that the presence of O is usually underestimated in EDS analyses. Magnetite (Fe_3O_4) showed a Fe:O ratio of about 2:3 instead of 3:4, while lepidocrocite and goethite (FeO_2H) showed a Fe:O ratio of 1:2 as expected, and finally, hydroxyapatite ($Ca_{10}P_6O_{26}H_2$) showed a Ca:P:O ratio of about 2:1:3 instead of 5:3:13.